

The Stretched-Mesh Huygens Absorbing Boundary Condition (SM-HABC)

Jean-Pierre Bérenger, *Fellow*, Hanan Almeer, Fumie Costen, *Senior Member*

Abstract—The Huygens absorbing boundary condition (HABC) is a new implementation of the analytical ABCs which were in common use before the introduction of the PML ABC. In contrast to the traditional implementation, the HABC allows analytical ABCs to be combined easily with other ABCs. This opens the way to combinations of two ABCs where the advantages of both are preserved while their drawbacks are removed. This is the case with the stretched mesh HABC which relies on an analytical ABC for the absorption of traveling waves and a real stretch of coordinates for the absorption of evanescent waves. This paper demonstrates that such a combination can achieve a high absorption over the whole frequency spectrum and can challenge the PML ABC in wave-structure interaction problems.

Index Terms—FDTD method, finite-difference, Huygens surface, absorbing boundary condition.

I. INTRODUCTION

Since its introduction [1], the Perfectly Matched Layer (PML) has been the most widely used absorbing boundary condition (ABC) in computational electromagnetics. However, some original ideas about ABCs have been published in the past decade. Among them are the multiple absorbing surfaces [2] and the re-radiating boundary condition [3], which were unified and generalized [4, 5] in the form of the Huygens absorbing boundary condition (HABC).

The HABC consists in canceling the outgoing field leaving a computational domain by means of equivalent currents that radiate a field equal in magnitude and opposite in sign to the field to be cancelled [4]. The equivalent currents are estimated by means of an operator of the same kind as the operators previously used with analytical ABCs [6], for instance the Higdon operators [7, 8]. As a consequence, the reflection from the HABC is the same as the reflection from the operator implemented as a traditional ABC [4]. From this, one may

think that the HABC is not an advance in comparison with analytical ABCs [6]. In particular, the poor performance of most analytical ABCs with regard to the absorption of evanescent waves is left unchanged. However, conversely to the analytical ABCs, the HABC can be placed in the inner domain, some distance from the outer boundary. This opens the way to easy combinations with other ABCs, for example with a PML [4].

The stretched-mesh HABC (SM-HABC) is such a combination of the HABC with another ABC, aiming to take advantage of the specific features of the two ABCs while removing their drawbacks. More specifically, the HABC absorbs the traveling waves, while the other ABC, denoted as SM, absorbs the evanescent waves. The SM ABC, presented here in the context of the finite-difference time-domain method (FDTD) [6], is not a really new ABC. It is just a strongly stretched FDTD mesh used to fill a large enough domain outside the HABC, in such a way that the evanescent waves can decrease to a negligible level. Stretched meshes were used in the past to reduce the overall number of FDTD cells while preserving a large physical domain. However, the stretching was severely limited when using ABCs on the outer boundary, because of the strong reflection of high frequencies from the large cells. Conversely, by placing the HABC in front of the stretched mesh, the high frequency traveling waves are absorbed by the HABC before entering the stretched mesh. Only evanescent waves are present behind the HABC, in the stretched domain. Since the evanescent waves are of low frequency, a strong stretch can be applied without penalty. The stretch can be so large that the stretched mesh can be reduced to a few FDTD cells while preserving a large enough physical domain. This permits the cost of the absorption of evanescent waves to be dramatically reduced.

Initially suggested as a possible idea of new and simple ABC [9], the SM-HABC has since been investigated [5, 10]. These preliminary studies showed that it can work very well, even better than was hoped initially [9]. The present paper reports more detailed investigations, in the context of the 3D FDTD method [6]. This paper addresses the interaction of waves with objects where high frequencies are traveling waves and low frequencies are evanescent waves, which allows strongly stretched meshes to be used. However, the content could be applied to other problems as well, since in the physical world evanescent waves are only present at low frequency in most problems.

Section II recalls the nature of the field radiated by a scattering object and Section III describes the implementation

Manuscript received xxxxxxxxxxxx.

F. Costen is with the School of Electrical and Electronic Engineering, the University of Manchester, M13 9PL, UK, and Image Processing Research Team, RIKEN, Center for Advanced Photonics, Saitama, Japan (e-mail: f.costen@cs.man.ac.uk).

H. Almeer is with the School of Electrical and Electronic Engineering, the University of Manchester, M13 9PL, UK (e-mail: almeer.h@gmail.com).

J.-P. Bérenger is currently a visiting professor at the School of Electrical and Electronic Engineering, the University of Manchester, M13 9PL, UK (e-mail: jpberenger@gmail.com).

of the SM-HABC. Section IV presents numerical experiments which demonstrate that the HABC relying on the first order Higdon operator can be placed close to a radiating object, and that stretched meshes can achieve high absorption of evanescent waves even with a large stretch. Section V reports numerical experiments with various canonical objects similar to the ones used in [11]. This permits the reader to compare with the most recently optimized CFS-PML. It appears that the SM-HABC can challenge the PML ABC in terms of the ratio between accuracy and computational cost.

II. PROBLEMS WITH EVANESCENT WAVES AT LOW FREQUENCY

In most problems of electromagnetics, the field is evanescent below a certain frequency. This is the case when an incident wave strikes a perfect electric conductor (PEC) body or any other complex object. The field surrounding the object is composed of evanescent waves at low frequency and traveling waves at high frequency, with a transition about the fundamental resonance of the object. Other problems are of the same nature, such as waveguide problems where the modes are evanescent below their cut-off frequency. In the following the features of the evanescent waves present around scattering structures are briefly summarized. They play an essential role in the principle of the SM-HABC.

Let us consider the general solution of the Maxwell equations in a vacuum, which is a special case of the solution derived in [12] in a PML. This is a plane wave in the form:

$$\psi = \psi_0 e^{j\omega \left[t - \frac{\cosh \chi}{c} X \right]} e^{-\frac{\omega}{c} \sinh \chi Y} \quad (1)$$

where ψ is any component of E or H fields, X is the direction of propagation of the phase, Y is the direction of the evanescence of the magnitude (perpendicular to X), χ is the evanescence coefficient, and ω is the angular frequency. In the special case $\chi = 0$, the solution (1) is a pure traveling wave. Consider now an object of size w struck by an incident wave. The field scattered by the object is composed of plane waves (1) where the coefficient ψ_0 of each wave depends on the problem conditions. At low frequency, far from the resonance corresponding to the largest size of the object w , the coefficient χ is connected to the frequency with a simple relationship. This was derived [12] as a consequence of the fact that the characteristic length of decay of the evanescent waves around a scattering object is of the order of its size. The relationship reads

$$\omega \sinh \chi = p \frac{c}{w} \quad (2)$$

where p is of the order of unity. Relation (2) has been found to be fruitful for the interpretation of the numerical reflection from PMLs [12], and it permitted effective CFS-PML to be designed [11, 13]. More recently, a theoretical derivation of (2) has been achieved in special cases [14]. In particular, with a symmetrical object (2) holds with $p = (2m + 1)\pi$, where m is a small integer. For the fundamental wave ($m=0$) we have $p = \pi$. In the following, a detailed knowledge of the waves around the objects is not needed. What is important is only the fact

that the characteristic length of the natural decrease of the evanescent waves is of the order of the size w of the object. This will permit the numerical reflection to remain small, even if the stretched cells are far larger than the uniform cells in the object region.

III THE SM-HABC

In principle, a HABC is a closed Huygens surface which radiates a field opposite to the outgoing field [4]. However, due to the discontinuities in the estimate of the outgoing field at its corners and edges, additional surfaces must be added to the closed surface [5]. These extensions rigorously cancel the spurious effect of the discontinuities (see details in [5]). The principle of the SM-HABC is then as depicted in Fig. 1. The scattering object is surrounded with a HABC and a large vacuum ended with a PEC condition is present behind the closed part of the HABC. The HABC absorbs the traveling waves while the large vacuum permits the evanescent waves to decrease naturally to an acceptable level.

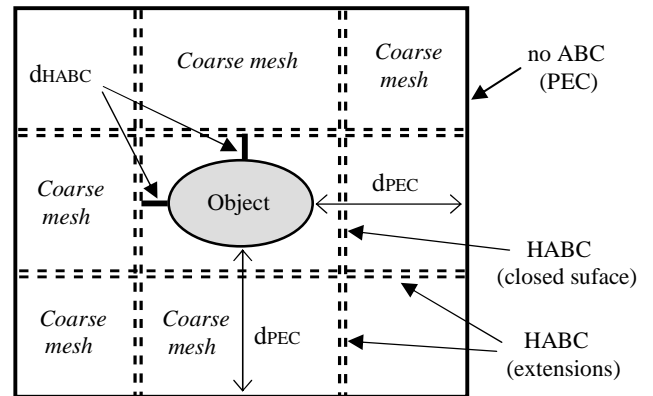


Fig. 1. The principle of the SM-HABC. The HABC is placed d_{HABC} from the object and the outer PEC d_{PEC} from the object.

In this paper the HABC relies on the first order Higdon operator [7, 8] which absorbs the traveling waves but reflects in totality the evanescent waves. It is shown that the HABC can be placed close to the object, i.e. the object-HABC separation d_{HABC} can be small in comparison with the object size. To allow the evanescent wave to decrease to an acceptable level, from Section II the separation d_{PEC} between the object and the outer PEC must be of the order of one or a few object sizes w . If the FDTD cells were uniform in the domain, the size of the exterior vacuum, in FDTD cells, would be prohibitive. However, only low frequency evanescent waves are present outside the HABC, and the characteristic length of their natural decrease is of the order of the object size. Therefore, the size of the cells can be strongly enlarged, i.e. the uniform mesh can be replaced with a strongly stretched mesh. This is demonstrated in the following sections by means of numerical experiments. The consequence is a dramatic reduction of the overall number of FDTD cells in comparison with the same overall volume filled with uniform cells.

IV NUMERICAL EXPERIMENTS WITH A 100-CELL OBJECT

The SM-HABC could be an effective ABC subject to two conditions:

1/ The HABC must absorb the traveling waves even when it is placed close to the scattering object, a few cells from the object with the FDTD method. This has never been investigated in the past since with traditional implementation the analytical ABCs were far from the object.

2/ The stretch of the mesh must be large, in order to greatly reduce the number of FDTD cells in the large vacuum exterior to the HABC. In other words, the reflection of evanescent waves must remain small even with large stretches.

The experiments provided in this section with a simple object show that the above two conditions hold. The object is a thin PEC plate of size 100x10 FDTD cells and zero thickness (Fig. 2). The FDTD cells are 1 cm in size, so the plate is 1 m in length, and the FDTD time step is 18 ps. Results are provided for two incident pulses, a Gaussian pulse [$\exp(-((t-t_0)/\tau)^2)$] where $\tau = 0.25$ ns and $t_0 = 2.5$ ns, and a unit-step pulse [$1-\exp(-t/t_{rise})$] where $t_{rise} = 1$ ns. With both pulses the incident wave is enforced by means of a Huygens surface [6] set one FDTD cell from the object.

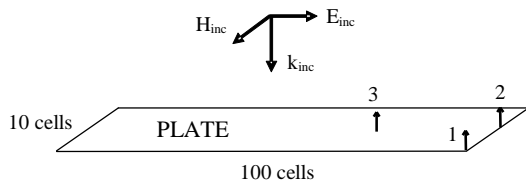


Fig. 2. The 100-10-cell PEC plate struck by an incident plane wave.

The overall size of the domain is such that the separation between the object and the exterior PEC condition equals two object size w . With the 1-meter 100-cell plate, the physical d_{PEC} in Fig. 1 equals 2 m, which is 200 FDTD cells if the mesh is uniform, or obviously a smaller number of cells if the mesh is stretched. The separation $d_{PEC} = 2w$ ensures a high natural decrease of the evanescent waves and then a small reflection of these waves into the inner domain where the object is present. From (1) and (2) the natural attenuation over $4w$ is $\exp(-4p)$, which yields reflections 0.0183 for $p = 1$ and $3.5 \cdot 10^{-6}$ for $p = \pi$ (-34.7 dB and -109.2 dB, respectively).

A. Experiments with a HABC and a large outer domain filled with a uniform mesh

Calculations were performed with a uniform FDTD cell (1 cm) and a separation $d_{PEC} = 200$ cells. The results are plotted in Fig. 3 for the two incident pulses, and for four locations of the HABC corresponding to separations $d_{HABC} = 3, 10, 30, 100$ cells. The field plotted in Fig. 3 is normal to the plate and half a cell above it, at point 1 in Fig. 2. A reference solution was computed using a large domain and a thick PML.

As can be observed, all the results are superimposed on the reference solutions. This confirms that the domain is large enough to permit the reflection of low frequency evanescent fields to be negligible. And this clearly demonstrates that a good absorption of the high frequency traveling waves can be

achieved by the HABC, even when it is as close as 3 FDTD cells from the object.

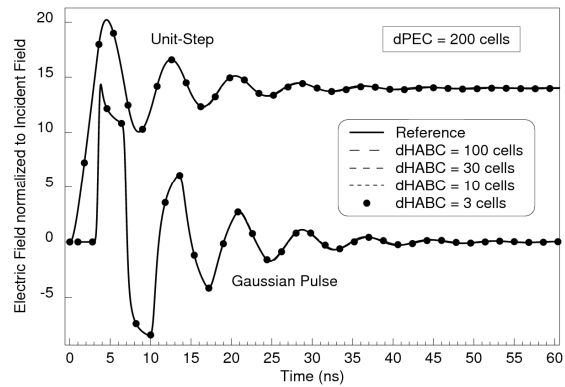


Fig. 3. Electric field on a 100-10-cell plate, at point 1 in Fig. 2, computed with the HABC placed 3, 10, 30, 100 cells from the plate, a uniform mesh in the whole domain, and the outer PEC 200 cells from the plate.

To demonstrate that the combination of the HABC with the large outer domain is needed to achieve the results in Fig. 3, two additional calculations were performed. In the first, the HABC was present ($d_{HABC} = 3$ cells), but the outer domain was reduced ($d_{PEC} = 20$ cells). In the second, the HABC was removed but the domain remained large ($d_{PEC} = 200$ cells). The results are reported in Fig. 4 for the unit-step incident wave. With the HABC and the small outer domain the late time plateau is strongly erroneous, which means that a large reflection of low frequency evanescent waves is present. Conversely, with the large domain but without HABC, the average value of the plateau is correct but spurious oscillations are present which means that high frequencies are not absorbed.

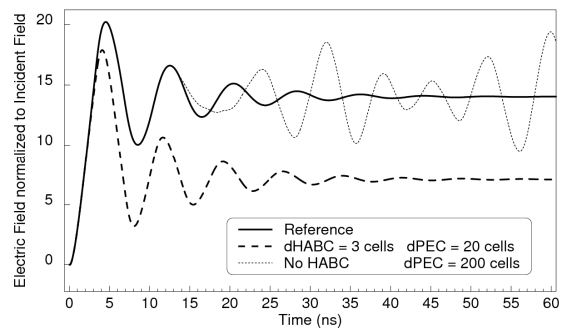


Fig. 4. Electric field on a 100-10-cell plate with a small outer domain and without HABC. The incident wave is the unit-step.

The need of the combination of the HABC with a large outer domain is also demonstrated in frequency domain in Fig. 5 where the Fourier transforms of Gaussian pulse results are plotted, with the HABC and a small domain, without HABC and with a large domain, and with the HABC and a large domain (the case $d_{HABC} = 3$ in Fig. 3). Fig. 5 is in accordance with Fig. 4. With the small domain the frequencies about and below the resonance are widely reflected, while without HABC the frequencies about and above the resonance are reflected in totality. With both the HABC and the large

domain, the two reflections are absent or negligible, even in the transition region which spans over one decade about the resonance.

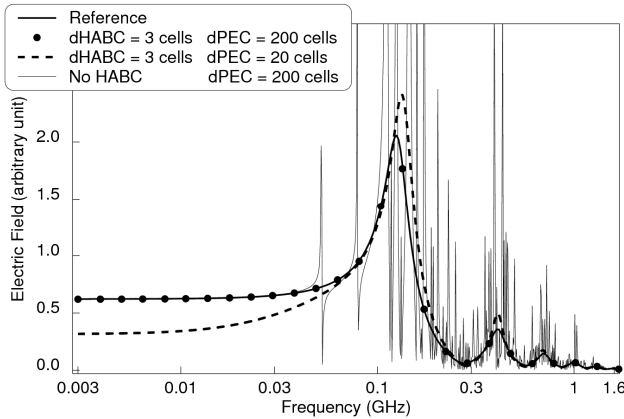


Fig. 5. Fourier transform of the electric field on a 100-10-cell plate, 1/ with HABC and a large domain ($d_{HABC} = 3$ cells case in Fig. 3), 2/ with HABC and a small domain, 3/ without HABC. Because the domain is lossless, an apodization was used to perform the Fourier transform without HABC.

In conclusion to the experiments in Figs. 3-5, the reflection of evanescent waves can be negligible if the domain is large enough, and the HABC relying on the first order Higdon operator can achieve a high absorption of the traveling waves, even when it is quite close to the object. Condition 1/ holds. This may appear as a little surprising since it was known that the operator ABCs must be placed far away from the objects to obtain correct solutions [6]. In fact, the large separation was needed to allow the evanescent waves to decrease. With the HABC, the absorptions of traveling waves and evanescent waves are decoupled. The Higdon operator is only devoted to the absorption of traveling waves. It does this very well, even if it is in the near vicinity of the object.

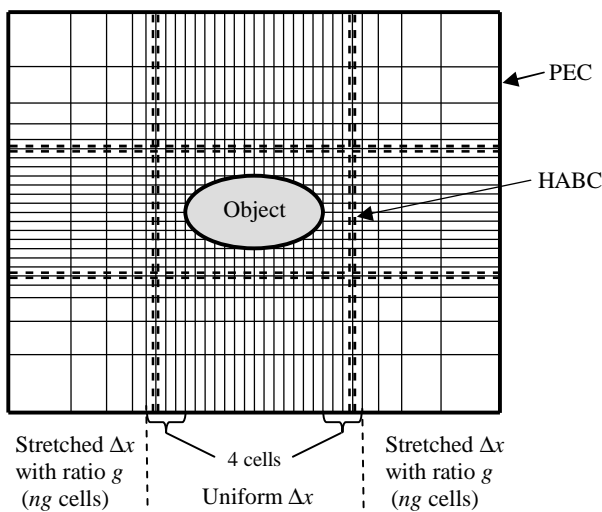


Fig. 6. The geometrical stretched mesh outside the HABC.

B. Experiments with a stretched mesh for the absorption of evanescent waves

In the experiments in Fig. 3, the computational domain is as large as the domain needed when using the traditional implementation of the operator ABC. The basic idea of the SM-HABC lies in the reduction of the number of FDTD cells in this domain while preserving its large physical size. This is achieved by using a stretched mesh. In this paper we use stretched meshes where the FDTD cell grows geometrically with ratio g , as represented in Fig. 6. The mesh is uniform in the central part, with four cells between the object and the beginning of the stretch. The HABC is placed in the uniform mesh, three cells from the object. The Huygens surface which radiates the incident wave is one cell from the object.

Two stretched meshes have been considered. Fig. 7 shows the successive sizes of the FDTD cells with the locations of the E and H planes (defining E planes in 3D FDTD as the planes holding two E nodes and one H node, and vice versa for the H planes). With mesh 1, the H planes are centred between E planes so that the ratio of distances between two successive planes (the size of half-cells) is not constant. With mesh 2, the ratio of distances between successive planes is constant, it equals $g^{1/2}$. E and H fields are then treated symmetrically. It is expected this could result in a better cancellation of the opposite numerical reflections produced by the E and H planes.

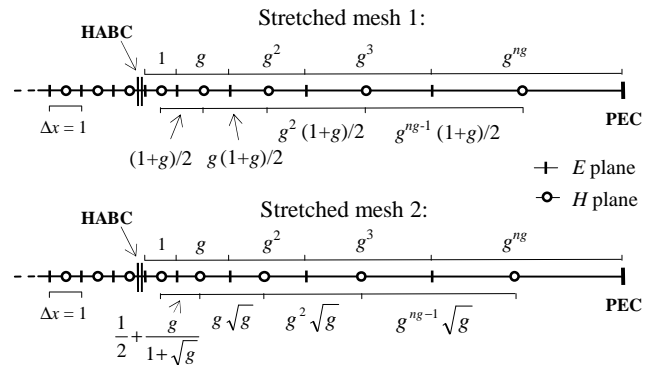


Fig. 7. The two geometrical stretched meshes. They differ with the locations of the H nodes.

Results computed with four stretched meshes are shown in Fig. 8. Parameter ng is the number of stretched cells. With for instance $ng = 10$, the separation between the plate and the outer PEC is composed of 4 uniform cells and 10 stretched cells. The ratio g is selected in order that the ng cells be equivalent to the $200 - 4 = 196$ uniform cells. This can be achieved using the formula which gives the number of uniform cells equivalent, in length, to ng stretched cells

$$ng_{equ} = g \frac{1 - g^{ng}}{1 - g} \quad (3)$$

Using (3) with $ng_{equ} = 196$, the values of g corresponding to $ng = 3, 5, 7, 10$ are 5.4400, 2.6140, 1.9159, 1.5265, respectively. The results in Fig. 8 were computed using mesh 1. Results of similar calculations with mesh 2 are plotted in Fig. 9. As expected, the symmetric mesh yields better results. With $ng =$

5 the results are about superimposed on the reference solution. Even with $ng = 3$ the results may be viewed as acceptable in some contexts (electromagnetic compatibility for instance).

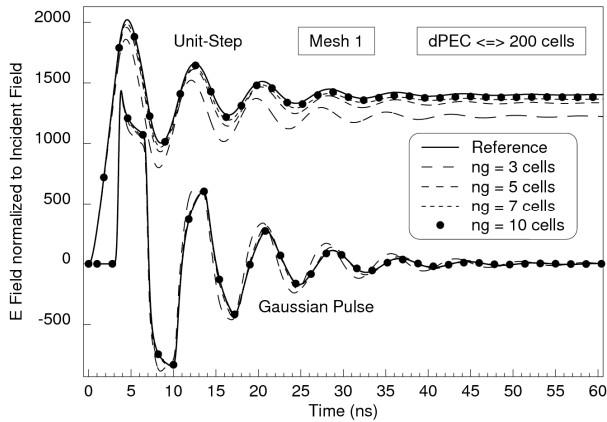


Fig. 8. Electric field on a 100-10-cell plate computed with the HABC 3 cells from the plate and four non-symmetric stretched meshes behind the HABC. In all cases the plate-PEC separation equals 2 m which is equivalent to 200 uniform cells.

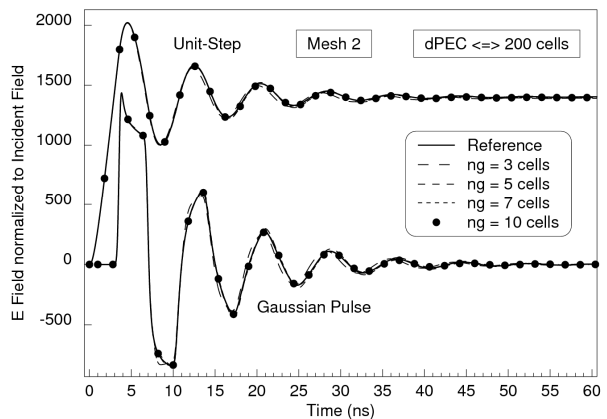


Fig. 9. Electric field on a 100-10-cell plate computed with the HABC 3 cells from the plate and four symmetric stretched meshes behind the HABC. In all cases the plate-PEC separation equals 2 m which is equivalent to 200 uniform cells.

The results in Figs. 8 and 9 show that correct results can be obtained with strongly stretched meshes and thus large FDTD cells between the HABC and the outer PEC. Consider for instance the case $ng = 5$. With ratio $g = 2.614$ the outer cell of the stretched mesh is 122 times larger than the cell in the central part. This is of the order of the object size (100 cells). Despite such large cells, the reflection remains small. This is rather better than was hoped. It was expected that the stretched cells could be far larger than the cells in the central part, but should remain smaller than the object size so as not to produce spurious reflection. Such an achievement is probably due, at least in part, to the cancellation of the opposite reflections from the E and H grid planes.

In order to demonstrate the difference between the HABC implementation of an operator and its traditional implementation, the experiments in Fig. 9 were re-run with the

same stretches of the mesh, but without HABC and with the Higdon operator implemented as an analytical ABC on the outer boundary. The results are plotted in Fig. 10. As expected the high frequencies are strongly reflected from the stretched mesh before they reach the outer boundary. Comparing Fig. 9 with Fig. 10 clearly demonstrates the dramatic improvement achieved by moving the Higdon operator from the outer boundary to the HABC placed in front of the stretched mesh.

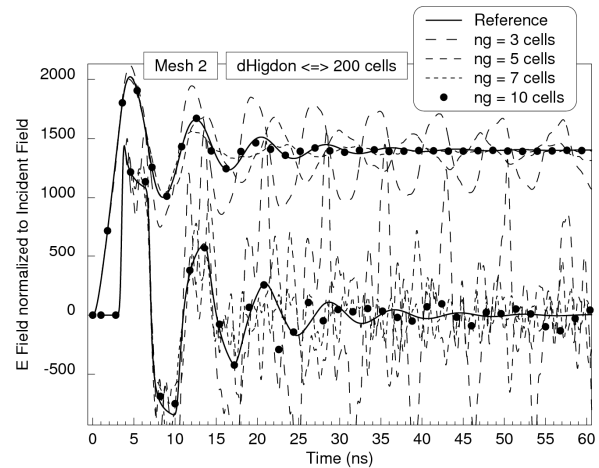


Fig. 10. Electric field on a 100-10-cell plate computed with four symmetric stretched meshes (the same as in Fig. 9) and a Higdon operator ABC placed on the outer boundary. In all the cases the plate-ABC separation equals 2 m which is equivalent to 200 uniform cells.

V NUMERICAL EXPERIMENTS WITH VARIOUS STRUCTURES

The experiments above have shown that the SM-HABC is quite effective with the 100-10-cell plate. In this section other experiments are reported with other canonical objects, namely a large 1000-100-1-cell plate, a 300-300-300-cell cube, an airplane structure 504-632-160 cells in size, and a 300-300-300-cell cube composed of human tissues.

The experiments were performed with two incident waves, the unit-step used in the sections above, which is the most challenging wave for the absorption of evanescent waves, and a double-exponential pulse $[\exp(-t/t_{fall}) - \exp(-t/t_{rise})]$, which is more representative of EMC applications, with $t_{rise} = 1$ ns and $t_{fall} = 100$ ns unless stated otherwise. The cell size was 1 cm and the time step 18 ps, except with the airplane.

As in the previous section the HABC is three cells from the objects which are surrounded by four uniform cells. Then, the mesh grows geometrically for ng cells. The stretched mesh is the symmetrical mesh 2 in Fig. 7 (the better one). The physical separation between the object and the outer PEC equals two times the size of the object, except with the cube.

C. A 1000-cell Plate

The object is a plate as in Fig. 2, but of size 1000-100 cells and of thickness one cell, that is a 1000-100-1-cell object. The E field normal to the plate is plotted in Fig. 11 at three points. The results are shown for four stretched meshes with 3, 5, 7, 10 cells, respectively, which replace $2000-4=1996$ uniform cells. Using (3) this is realized with ratios $g = 12.240, 4.339, 2.779, 1.995$, respectively. As can be seen, the results are close

to the reference solution even with $ng = 5$. In that case, the outer PEC is only $4 + 5 = 9$ cells from the object.

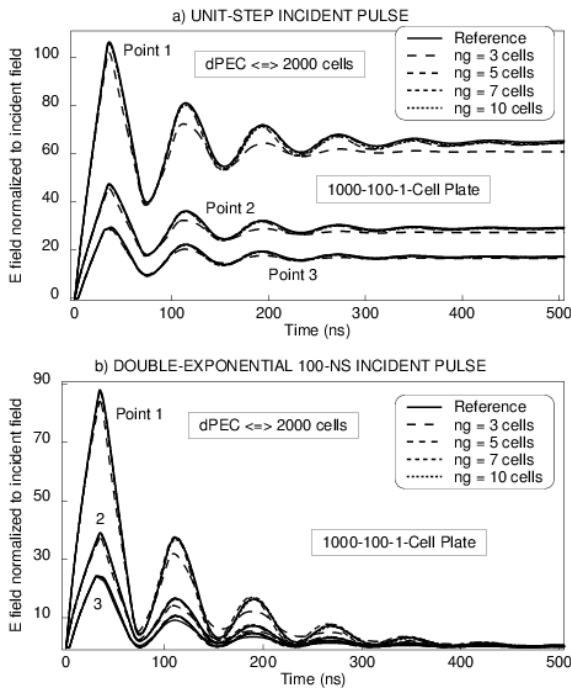


Fig. 11 Electric field on the surface of a 1000-100-1-cell PEC plate with the SM-HABC of 3, 5, 7, 10 stretched cells. Points 1, 2, 3 are at locations represented in Fig. 2. The incident wave is either a unit-step (upper part) or a double-exponential pulse (lower part).

Comparing Fig. 11 with Fig. 8 in [11] shows that the computational requirements of the SM-HABC are similar to those of the optimized CFS-PML. Consider for instance the cases with the 5-cell PML and the $ng = 7$ SM-HABC which yield similar results (both are superimposed on the reference solution). With the PML there are $2 + 5 = 7$ cells around the plate (the PML is 2 cells from it), and with the HABC, $4 + 7 = 11$ cells. However, since the cost (CPU time and memory) of one cell of PML is larger than the cost of one cell of vacuum (or stretched mesh), the costs of the two techniques of simulation of free space are quite similar.

D. A 300-cell Cube

From previous researches on ABCs [11]-[13], the cube is one of the most challenging structures for the absorption of evanescent waves. Results of experiments with a 300-cell cube are provided in Fig. 12 with stretched meshes of lengths 3, 5, and 7 cells.

Converse to previous experiments where d_{PEC} between the object and the outer PEC was two object sizes w , in Fig. 12 $d_{PEC} = 4w$, which is equivalent to 1200 uniform cells. Initially, the calculations were performed with $d_{PEC} = 2w$. The results slightly differed from the reference solution, especially the plateau of the unit-step solution, even when widely increasing the number ng of cells of the stretched mesh. This is because the distance between the centers of the opposite sides of the cube equals $w/2 + w + w/2$. The period of resonance is then close to that of a thin object of length $2w$. Therefore, the decrease

of the evanescent waves is similar to that of a thin object $2w$ in size. Calculations were re-run with $d_{PEC} = 4w$ and $6w$. As expected, the solution approaches the reference when d_{PEC} is growing. With $d_{PEC} = 4w$ (Fig. 12) it is quite close to the reference.

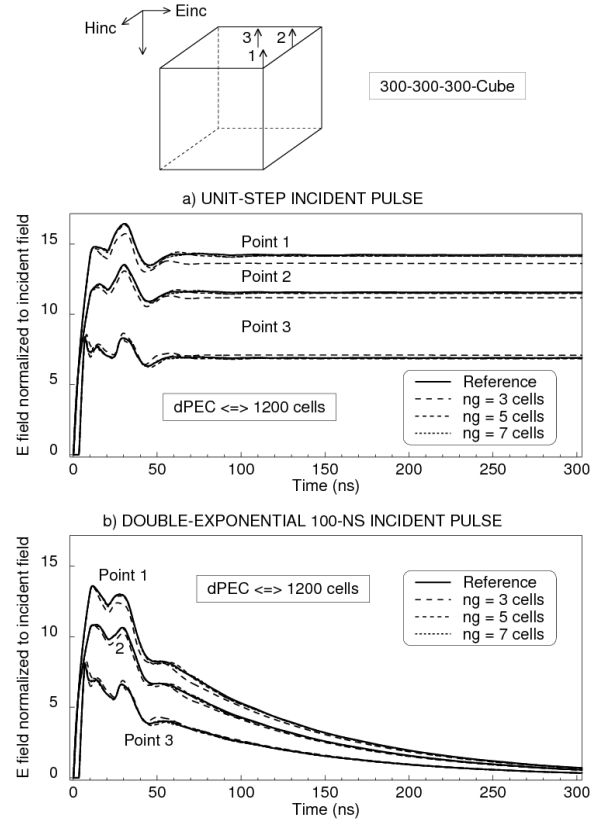


Fig. 12. Electric field on the surface of a 300-cell cube for the unit-step and double-exponential pulses when $d_{PEC} = 4w$. The fields at points 2 and 3 are multiplied by 2 and 20, respectively.

Finally, even if a larger separation d_{PEC} is needed for the cube than for the plate, again accurate solutions can be obtained with a few stretched cells, rendering the SM-HABC close to the CFS-PML in terms of computational requirements. This can be seen by comparing with Fig. 9 in [11].

E. A 504-632-160-cell Airplane Structure

This experiment is with an airplane structure of size $31.5 \times 39.5 \times 10.0$ meters discretized with FDTD cells of 6.25 cm. As with previous objects, the HABC is 3 cells from the airplane and there are four uniform cells around the object (more precisely around the parallelepiped that just fits the airplane). However, even with only four cells between the stretched mesh and the end of the wings, the fuselage, and the drift, there is an important amount of vacuum between most of the PEC surface and the stretched mesh. This permits the evanescent waves to decay before striking the stretched mesh. Thus, we expect better results than in the cases with the plate or the cube. This is well verified in Fig. 13. In particular, even

with a 3-cell stretched mesh the results match the reference solution with the double-exponential pulse.

Again, comparing Fig. 13 with Fig. 10 in [11] shows that the SM-HABC can achieve a similar accuracy as the CFS-PML with similar computational requirements. For instance the cases with the 4-cell PML in [11] and with the 5-cell SM-HABC here (6 cells and 9 cells in total, respectively, but cells with the SM-HABC are less costly).

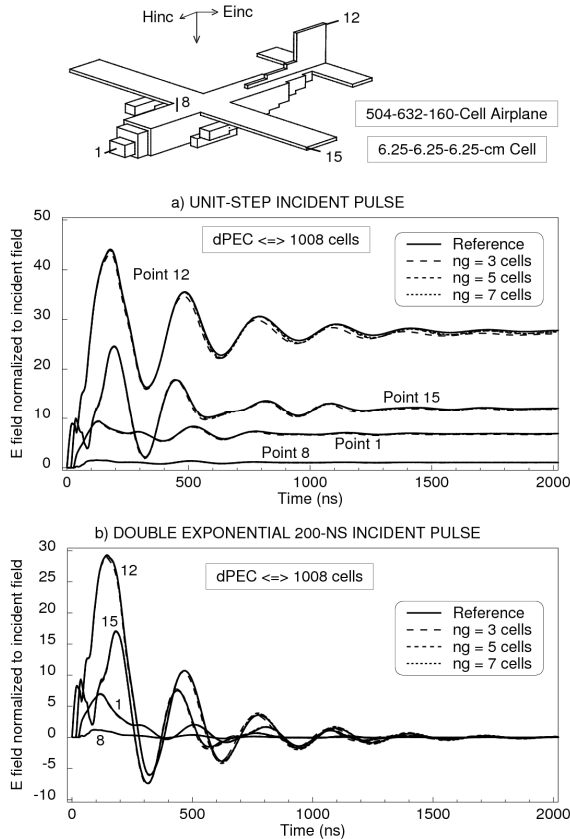


Fig. 13. Electric field on the surface of a 504-632-160-cell airplane with SM-HABC of 3, 5, 7 stretched cells, for a unit-step and a double-exponential pulse.

F. A human-tissue 300-cell cube

In this experiment, the scattering structure is a penetrable object composed of human tissues. The object is a 280-cell cube of Fat surrounded with a 10 cell thick layer of Skin. This forms a 300-cell cube of size 60 cm (2-mm and 3.6-ps FDTD steps). The human tissues are assumed as Debye media where the relative permittivity reads:

$$\epsilon_r(\omega) = \epsilon_\infty + \frac{\epsilon_s - \epsilon_\infty}{1 + j\omega\tau} + \frac{\sigma}{j\epsilon_0\omega} \quad (4)$$

where ϵ_s , ϵ_∞ , τ , σ , are the static permittivity, the optical permittivity, the relaxation time, and the conductivity.

In the Debye media, the FDTD solution [15] consists of solving the Maxwell equations for D and H fields and then obtaining the E field from D at every E - D node by discretizing the time domain counterpart of (4).

The incident wave was the pulse $100 [\exp(-((t-5\tau)/\tau)^2)]$ V/m with $\tau = 0.5$ ns, striking the cube as in Fig. 12. Fig. 14 shows the E field parallel to the incident E at the center of the cube, computed with $d_{PEC} = 2w$ and 3, 5, 10 stretched cells. As with PEC objects, the solution rapidly tends to a limit as ng grows. This suggests that a small number of stretched cells permits the correct simulation of free space to be achieved around penetrable objects. However, the structure of the evanescent fields around such objects is not as well known as that around PEC objects [14]. Therefore, further studies remain to be performed to confirm such preliminary results.

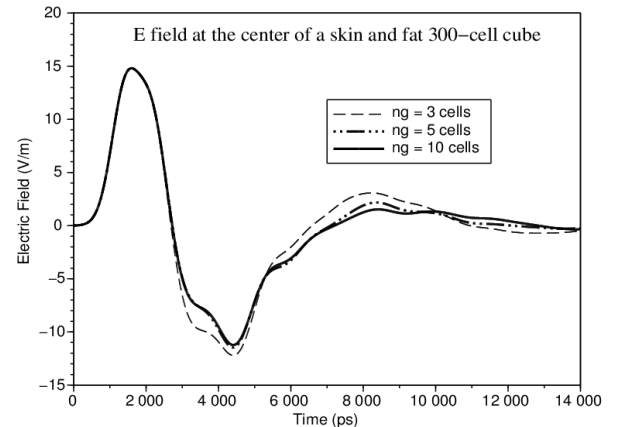


Fig. 14. Electric field at the center point of a 300-cell cube composed of Skin ($\epsilon_s = 47.93$, $\epsilon_\infty = 29.85$, $\tau = 4.36 \cdot 10^{-11}$ s, $\sigma = 0.541$ mho/m) and Fat ($\epsilon_s = 5.53$, $\epsilon_\infty = 4.00$, $\tau = 2.36 \cdot 10^{-11}$ s, $\sigma = 0.037$ mho/m).

VI. CONCLUSION

The HABC concept [2-5] has revolutionized the use of the analytical ABCs as it permits easy combinations of an analytical ABC with any other ABC. The SM-HABC, which combines a Higdon operator with a real stretch of coordinates, is just one of the numerous combinations that can be imagined. It has been demonstrated in this paper that it can achieve high absorption of electromagnetic waves over the whole spectrum, including low frequency evanescent waves. Its effectiveness is close to that of the optimized CFS-PML ABC in wave-structure interaction problems.

Even if its performance is high, further improvements to the SM-HABC are currently under investigation. These include the replacement of the first order Higdon operator with a higher order operator to improve the absorption of traveling waves, and the optimization of the profile of the stretch of coordinate to further reduce the reflection of evanescent waves. Moreover, application of the SM-HABC to other problems can be envisaged. It is obvious, for example, that the SM-HABC is well suited to the termination of waveguides where evanescent waves are only present at low frequencies.

REFERENCES

- [1] J.-P. Bérenger, "A perfectly Matched Layer for the Absorption of Electromagnetic Waves", *J. Comput. Phys.*, vol. 114, pp. 185-200, 1994.

- [2] I. Wayan Sudiarta, "An absorbing boundary condition for FDTD truncation using multiple absorbing surfaces", *IEEE Trans. Antennas Propag.* 51 (2003), 3268-3275.
- [3] R.E. Diaz, I. Scherbatko, "A simple stackable re-radiating boundary condition (rRBC) for FDTD", *IEEE Antenna Propag. Magazine* 46 (1) (2004) 124-130.
- [4] J-P. Bérenger, "On the Huygens absorbing boundary conditions for electromagnetics", *J. Comput. Phys.* (2007) doi: 10.1016/j.jcp.2007.04.008176-190.
- [5] F. Costen, J.-P. Bérenger "Implementation of the Huygens absorbing boundary condition in corner regions" *IEEE Trans. Electr. Compat.*, vol. 54, no. 2, pp. 367-374, Apr. 2012. doi: 10.1109/TEMC.2012.2186302.
- [6] A. Taflove, S. Hagness, "Computational electrodynamics: The finite-difference time-domain method", Artech House 2005.
- [7] R. Higdon, Absorbing boundary conditions for difference approximations to the multi-dimensional wave equation, *Math. Comput.* 47 (1986) 437-459.
- [8] R. Higdon, "Numerical absorbing boundary conditions for the wave equation", *Math. Comput.* 49 (1987) 65-90.
- [9] J.-P. Bérenger "Approaching the ideal absorbing boundary condition" *IEEE AP-S Int Symp.*, Charleston, USA, June 1-5, 2009.
- [10] J.-P. Bérenger, F. Costen, "Application of the Huygens absorbing boundary condition to wave-structure interaction problems", *IEEE AP-S Int. Symp.*, Toronto, Canada, July 12-16, 2010.
- [11] J.-P. Bérenger "An optimized CFS-PML for wave-structure interaction problems" *IEEE Trans. Electr. Compat.*, vol. 54, no. 2, pp. 352-358, Apr. 2012. doi: 10.1109/TEMC.2011.2178852.
- [12] J.-P. Bérenger "Evanescence waves in PML's: Origin of the numerical reflection in wave-structure interaction problems" *IEEE Trans. Antennas Propag.*, vol. 47, no. 10, pp. 1497-1503, Oct. 1999.
- [13] J.-P. Bérenger, "Numerical Reflection from FDTD-PML's: A Comparison of the Split PML with the Unsplit and CFS PML's", *IEEE Trans. Antennas Propag.*, vol. 50, pp. 258-265, 2002.
- [14] J.-P. Bérenger " On the general solution of the Maxwell equations and the impact on the absorbing boundary conditions. Workshop "Present challenges in electromagnetic modelization", Saint-Malo, France, December 2-3, 2010.
- [15] M. Abalenkovs, F. Costen, J.-P. Bérenger , R. Himeno, H. Yokota, M. Fujii " Huygens Subgridding for 3D Frequency-Dependent Finite-Difference Time-Domain Method". *IEEE Trans. Antennas Propag.*, vol. 60, pp. 4336-4344, 2012.



Hanan Almeer received a BSc and a MSc in computer engineering from Kuwait University, Kuwait. Since 2011, she has been doing her PhD in the high performance computing and the computational electromagnetics in the University of Manchester, UK. Her domain of interest is Parallel Computing. In her PhD she accelerated the computations of the FDTD method with the Absorbing Boundary Conditions using CUDA on GPUs and OpenMP on CPUs.



Fumie Costen received a BSc, a MSc in Electrical Engineering and a PhD in Informatics, all from Kyoto University, Japan. From 1993 to 1997 she was with Advanced Telecommunication Research International, Kyoto, Japan, where her domain of interest was Direction-Of-Arrival estimation based on MUSIC algorithm for three-dimensional laser microvision. She received an ATR Excellence in Research Award in 1996, an academic invitation at Kiruna Division, Swedish Institute of Space Physics, Sweden in 1996 and gained three patents in 1999 from the work. From 1998 to 2000, she was with Manchester Computing in the University of Manchester, U.K., where she was engaged in the research on metacomputing. She received a best paper award from 8th International Conference on High Performance Computing and Networking Europe in 2000. Since 2000, she has been a lecturer in the University of Manchester, U.K. Her main field of interest is the computational electromagnetics in such topics as a variety of the finite difference time domain methods for low frequency and high spatial resolution and FDTD subgridding and boundary conditions. Her work extends to the hardware acceleration of the computation using GPGPU, SSE and AVX instructions.



Jean-Pierre Bérenger (F'09) received a Master in Physics from the University Joseph Fourier, Grenoble, France, in 1973, and a Master in Optical Engineering from the Institut d'Optique Graduate School, Paris, France, in 1975.

From 1975 to 2013 he was with the Direction Générale de l'Armement of France, where he was a research engineer on the electromagnetic effects of nuclear rays (1975-1989), he held a position as expert on the electromagnetic effects of nuclear events

(1989-1998), and he was a contract manager while staying active in the field of numerical electromagnetic (1998-2013). He is currently a consultant on electromagnetic effects of nuclear rays and on numerical electromagnetics, and a visiting professor at the School of Electrical and Electronic Engineering, the University of Manchester, UK. His researches include low frequency propagation, absorbing boundary conditions, and FDTD method. He is a member of the Electromagnetics Academy and has been an Associate Editor of the IEEE Transactions on Antennas and Propagation from 2006 to 2010. He received the 2013 Medal of URSI-France.